



# Soluble 4R0N Tau Abrogates Endocytic Vesicular Dynamics

Tharun Selvam Mahendran<sup>1</sup>, S. N. Suresh<sup>2</sup>, Lakshmi Garimella<sup>1</sup> and Ravi Manjithaya<sup>1,3\*</sup>

<sup>1</sup>Molecular Biology and Genetics Unit, Jawaharlal Nehru Centre for Advanced Scientific Research, Bangalore, India, <sup>2</sup>Centre for Brain Research, Indian Institute of Science, Bangalore, India, <sup>3</sup>Neuroscience Unit, Jawaharlal Nehru Centre for Advanced Scientific Research, Bangalore, India

Aggregated tau is a hallmark neuropathological feature in numerous neurodegenerative disorders. Previous studies aiming to validate aggregated tau pathology as a pathogenic driver of neurodegeneration in correlation to characteristic behavioral phenotypes have had shortcomings. Although studies on soluble tau pathology have effectively addressed these shortcomings, the role of soluble tau in the molecular pathogenesis of neurodegeneration is not yet unequivocally established. In sporadic Alzheimer's disease (AD), the relevance of soluble tau pathology in endolysosomal dysfunction and autophagic stress, some of the earliest disease manifestations, is unclear. In this study, we report that soluble 4R0N tau overexpression affects the expression levels of certain markers associated with the endolysosomal system and autophagy. Moreover, through live-cell imaging, we found that the vesicular dynamics of early endosomes were affected with respect to spatiotemporal parameters and vesicle maturation. Additionally, we observed the localization of amyloid precursor protein (APP) along the endocytic pathway and found that upon overexpression of soluble 4R0N tau, APP was preferentially localized to the endocytic compartments implicated in the amyloidogenic pathway. Overall, our observations indicate that soluble 4R0N tau abrogates the dynamics of the endolysosomal system, autophagy, and affects the trafficking of APP. Since the amyloidogenic processing of APP occurs during its progression through the endocytic pathway, our results suggest that the generation of amyloid- $\beta$  ( $A\beta$ ) might also be modulated.

## OPEN ACCESS

### Edited by:

Elena Tamagno,  
University of Turin, Italy

### Reviewed by:

Fernando Goni,  
New York University, United States  
Gunnar Keppeler Gouras,  
Lund University, Sweden

### \*Correspondence:

Ravi Manjithaya  
ravim@incasr.ac.in

**Keywords: Alzheimer's disease, vesicular trafficking, amyloid precursor protein (APP), endosome dysfunction, autophagic stress, soluble 4R0N tau, endocytic dysfunction, vesicle tracking**

**Received:** 25 February 2020

**Accepted:** 18 September 2020

**Published:** 05 November 2020

### Citation:

Mahendran TS, Suresh SN,  
Garimella L and Manjithaya R  
(2020) Soluble 4R0N Tau Abrogates  
Endocytic Vesicular Dynamics.  
*Front. Aging Neurosci.* 12:537712.  
doi: 10.3389/fnagi.2020.537712

## INTRODUCTION

Tau is an intrinsically disordered proteinaceous cytoskeletal element known to associate with microtubules and bundle actin filaments (Weingarten et al., 1975; He et al., 2009; Morris et al., 2011), and it is highly expressed in the human central nervous system as six major isoforms *via* alternative splicing (Mandelkow and Mandelkow, 2012). In a physiological context, tau remains soluble and functional, but in the case of idiopathic neurodegenerative disorders such as sporadic Alzheimer's disease (AD), elevated levels of tau (Khatoun et al., 1992) become highly susceptible to conformational changes, aggregation, and oligomerization and further

assembly into paired helical filaments (PHFs), which then nucleate into neurofibrillary tangles (NFTs; Wille et al., 1992; Crowther et al., 1994; Wilson and Binder, 1995; Patterson et al., 2011). For simplicity, we shall refer to pathological tau conformers including oligomers, PHFs, and NFTs as tau aggregates. Gain-of-function toxicity of tau has been implicated in the pathogenesis of AD, which is predominantly characterized by the presence of pathological protein aggregates such as tau aggregates and amyloid- $\beta$  ( $A\beta$ ) containing senile plaques (Mitchell et al., 2002; Maeda et al., 2006; Johnson et al., 2016; Schöll et al., 2016). This toxicity was presumably attributed to aggregated tau formed by the nucleation events involving soluble tau, mediated by liquid–liquid phase separation (Ambadipudi et al., 2017; Wegmann et al., 2018). However, there is a lack of evidence to unequivocally establish which aggregated state(s) of tau has a role in the cascade of events leading to neurodegeneration.

The presence of aggregated tau in the brains of transgenic mice was found to be correlated with behavioral and electrophysiological abnormalities as well as neuronal loss, characteristic of clinical AD pathology. Upon closer analysis, when the expression level of tau, that is yet to aggregate, was reduced later in the lifespan of these mice, some of the initially observed AD pathology-related phenotypes were ameliorated despite the prevalence of tau aggregates (Santacruz et al., 2005). These observations imply that tau in a soluble form, rather than the end-point aggregated form, is responsible for AD pathology-related phenotypes. In accordance with the previous observations, several studies have revealed that soluble tau is responsible for neuronal loss through the activation of caspases as well as synaptic dysfunction that underlies cognitive impairment (Spires-Jones et al., 2008; de Calignon et al., 2010; Bolós et al., 2017). Furthermore, transgenic mice engineered to overexpress tau with a high propensity to aggregate, do not successfully mirror behavioral and histopathological phenotypes observed in AD-related clinical studies (McGowan et al., 2006; Dawson et al., 2018; Strang et al., 2018).

The pathological relevance of soluble tau in AD pathology has been demonstrated by multiple studies, as mentioned earlier. However, the role of soluble tau in the pathogenesis of AD is still unclear. Many studies have reported correlations between pathologies of soluble tau and  $A\beta$  thereby hinting toward possible crosstalk. In the case of neuropathology, accumulation of soluble tau has been shown to precede that of  $A\beta$  plaque deposition, and it also correlates well with aging (Braak et al., 2011). A study involving electrophysiology showed that soluble tau-induced silencing of neuronal activity overshadowed  $A\beta$ -induced neuronal hyperactivity, indicating that tau pathology was more impactful than that of  $A\beta$  (Busche et al., 2019). Moreover, soluble tau pathology exacerbates  $A\beta$ -induced neurotoxicity in AD-related transgenic mice (Roberson et al., 2007; Ittner et al., 2010). More direct correlations between soluble tau and  $A\beta$  pathologies have also been demonstrated in recent years. Soluble tau pathology can potentially drive  $A\beta$  production directly through the STAT1–BACE1 axis (Zhang et al., 2018). Passive immunization of AD transgenic mice with antibodies against tau, resulted in a reduction in the total  $A\beta$

burden, indicating a potential cross-talk between soluble tau and the amyloidogenic pathway, which gives rise to  $A\beta$  (Dai et al., 2017). Collectively, these studies hint that tau could be playing an upstream role relative to  $A\beta$  in the progression of AD pathogenesis.

However, a direct connection between soluble tau pathology and the production of  $A\beta$  is lacking. Since  $A\beta$  generation primarily occurs at the endocytic compartments due to the interaction between amyloid- $\beta$  precursor protein (APP) and  $\beta$ -secretase (BACE1; Rajendran et al., 2006; Das et al., 2015), we hypothesized that soluble tau pathology could contribute to  $A\beta$  generation through disruption of endocytic vesicular dynamics. Hence, we designed this study to elucidate the effect of soluble tau on endocytic vesicular dynamics and trafficking of APP along the endocytic pathway. Such an endeavor will require close attention to the major compartments of the endolysosomal system such as the early endosomes, late endosomes, and lysosomes labeled with the RAB/LAMP protein markers. As the model for our study, we have used HeLa cells with episomal overexpression of 4R0N tau (soluble 4R0N tau; Hoover et al., 2010), which is an alternatively spliced variant of tau that contains four repeats of the microtubule-binding domain without the N-terminal sequence and contains exons 1, 4 and 5, 7, and 9–13, intron 13, and exon 14. The endolysosomal system of HeLa does not operate in a complex regulatory manner such as that observed in certain specialized cell types with very dynamic membrane/vesicle homeostasis, thereby allowing for highly interpretable readouts of the endocytic vesicular dynamics (Parton et al., 1992; Overly and Hollenbeck, 1996; Nixon, 2005). Moreover, HeLa cells do not show a detectable level of tau mRNA transcripts, which minimizes the chances of observing overexpression artifacts during experimentation with the 4R0N tau plasmid construct (Thul et al., 2017). In addition, the relatively symmetric morphology of HeLa cells enables highly robust and reproducible computational analysis of endocytic vesicular dynamics without the need for manual segmentation for different cell regions. For the ease of quantitative analysis and a lesser degree of variability, we opted to use HeLa as the model for our study.

The current study aims to understand the *in cellulo* effect of soluble 4R0N tau overexpression on the endolysosomal system and trafficking of APP as a cargo. In our study, we show that overexpression of soluble 4R0N tau correlates with impaired endolysosomal flux, induction of autophagic stress, and enhanced sequestration of APP into endocytic compartments, which can potentially stimulate the amyloidogenic pathway.

## MATERIALS AND METHODS

### Chemicals and Antibodies

Anti-rabbit IgG Atto 633 (41176), anti-mouse IgG Atto 633 (78102), and trypsin-EDTA (59418C) were purchased from Sigma–Aldrich (St. Louis, MO, USA). Anti-rabbit IgG antibody conjugated with horseradish peroxidase (7074), anti- $\beta$ -actin antibody (4970), anti-LAMP1 antibody (9091), anti-RAB5 antibody (3547), and anti-RAB7 antibody (9367) were

purchased from Cell Signaling Technology (Danvers, MA, USA). Beclin-1 (sc-48341) antibody was purchased from Santa Cruz Biotechnology (Dallas, TX, USA). Anti-mouse IgG antibody conjugated with horseradish peroxidase (172-1011) was purchased from Bio-Rad (Hercules, CA, USA). Plasmid miniprep kit was purchased from Qiagen (Hilden, Germany).

## Plasmid Constructs

Plasmids used for the experiments include pRK5-EGFP-tau (hereafter 4R0N tau or soluble 4R0N tau; gift from Karen Ashe; Addgene, 46904; Hoover et al., 2010), pEGFP-N1 (hereafter vector control or control; 6085-1, Clontech), mCh-RAB5 (gift from Gia K. Voeltz; Addgene, 49201; Friedman et al., 2010), pmRFP-LC3 (gift from Tamotsu Yoshimori; Addgene, 21075; Kimura et al., 2007), pDsRedm-C1:APP (gift from Prof. Erika Holzbaur, University of Pennsylvania, Philadelphia, PA, USA; Fu and Holzbaur, 2013). All of the plasmid constructs used in the study were validated by DNA sequencing and immunoblot analysis prior to experimentation (data not shown).

## Transfection

HeLa cells were seeded such that the cultured cells reached 50–60% confluency by the following day for transfection. Transfection of HeLa cells with the appropriate plasmids was conducted using the Lipofectamine 2000 transfection reagent (11668-019, Life Technologies, Carlsbad, CA, USA) in accordance with the manufacturer's instructions. All cell culture-related experiments were performed 48 h after transfection.

## Cell Culture

HeLa cells were maintained in Dulbecco's modified Eagle medium (DMEM; Sigma-Aldrich, D5648) supplemented with 3.7 g/l of sodium bicarbonate (Sigma-Aldrich, S5761), 10% fetal bovine serum (FBS; PAN, 3302-P121508), and 100 U/ml of penicillin and streptomycin (Sigma-Aldrich, P4333). The cells were maintained at 37°C in a humidified atmosphere with 5% CO<sub>2</sub>. For immunofluorescence experiments, subconfluent HeLa cells were seeded in 60-mm dishes containing coverslips and incubated overnight. Subsequently, cells were transfected with the respective plasmids and incubated for 48 h until they were processed for microscopy. For live-cell imaging-related experiments, subconfluent HeLa cells were seeded in coverslip bottom cell-imaging dishes (0030740017, Eppendorf, Hamburg, Germany). Cells were transfected with the respective plasmids, then incubated for 48 h and imaged. For the immunoblotting experiments, HeLa cells were seeded in six-well dishes and incubated overnight. Cells were then transfected with the respective plasmids, incubated for 48 h, and subsequently processed for immunoblot experiments.

## Immunofluorescence

After 48 h of transfection, HeLa cells seeded on coverslips were washed with 1× PBS, fixed with 4% paraformaldehyde (Sigma-Aldrich, P6148), and then permeabilized with 0.25% Triton X-100 (MB03, HiMedia Laboratories, Mumbai, India) followed by incubation with the respective primary antibody, overnight at 4°C. The primary antibodies were diluted appropriately in 0.25% BSA in 1× PBS. After primary antibody

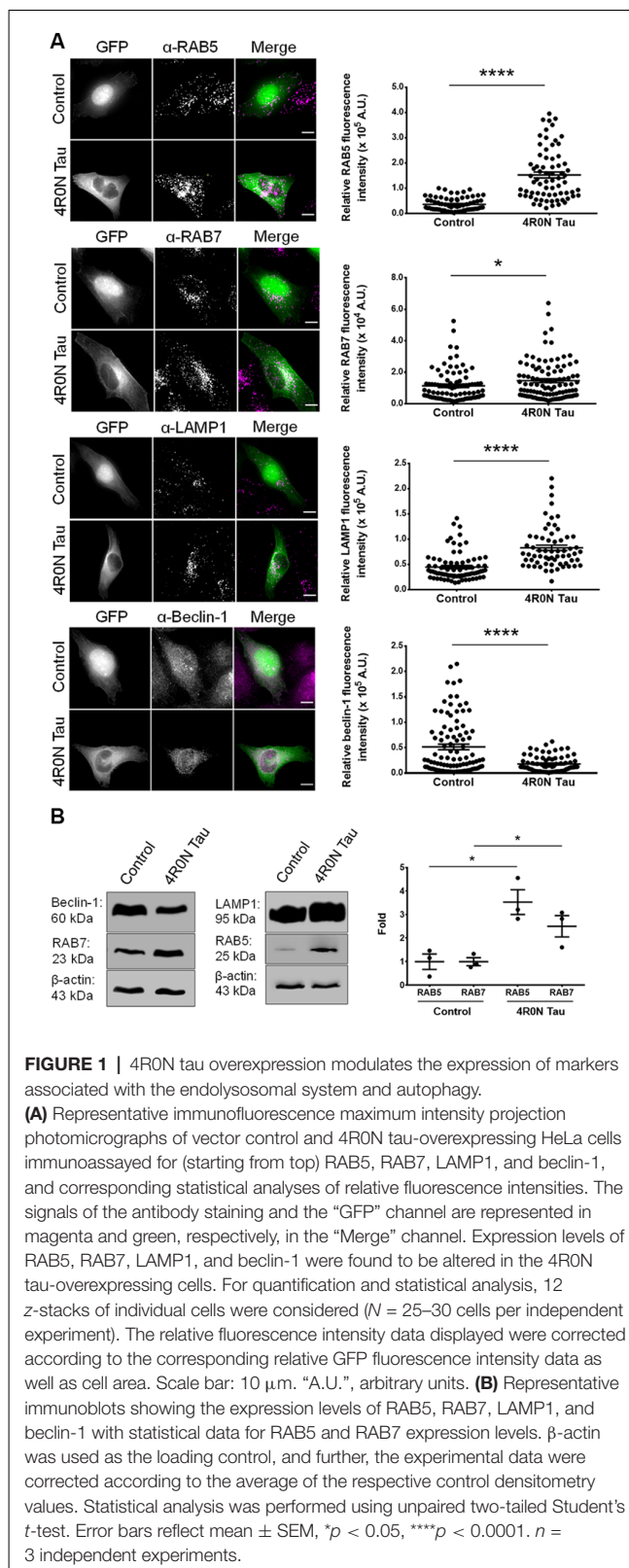


**FIGURE 1** | 4R0N tau overexpression modulates the expression of markers associated with the endolysosomal system and autophagy.

**(A)** Representative immunofluorescence maximum intensity projection photomicrographs of vector control and 4R0N tau-overexpressing HeLa cells immunostained for (starting from top) RAB5, RAB7, LAMP1, and beclin-1, and corresponding statistical analyses of relative fluorescence intensities. The signals of the antibody staining and the “GFP” channel are represented in magenta and green, respectively, in the “Merge” channel. Expression levels of RAB5, RAB7, LAMP1, and beclin-1 were found to be altered in the 4R0N tau-overexpressing cells. For quantification and statistical analysis, 12 z-stacks of individual cells were considered ( $N = 25\text{--}30$  cells per independent experiment). The relative fluorescence intensity data displayed were corrected according to the corresponding relative GFP fluorescence intensity data as well as cell area. Scale bar: 10  $\mu\text{m}$ . “A.U.,” arbitrary units. **(B)** Representative immunoblots showing the expression levels of RAB5, RAB7, LAMP1, and beclin-1 with statistical data for RAB5 and RAB7 expression levels.  $\beta$ -actin was used as the loading control, and further, the experimental data were corrected according to the average of the respective control densitometry values. Statistical analysis was performed using unpaired two-tailed Student's *t*-test. Error bars reflect mean  $\pm$  SEM, \* $p < 0.05$ , \*\*\*\* $p < 0.0001$ .  $n = 3$  independent experiments.

incubation, the coverslips were incubated with the appropriate secondary antibody for 2 h at RT. The appropriate secondary antibody dilutions were made in 0.25% BSA in 1× PBS. The

coverslips were mounted on slides using Vectashield mounting medium (H-1,000, Vector Laboratories, Burlingame, CA, USA).

## Immunoblotting

After 48 h of transfection, the cells were washed with 1× PBS, scraped, and collected in standard Laemmli buffer. The lysates were boiled for 10 min at 95°C. The lysates were then subjected to SDS-PAGE and subsequently transferred onto a PVDF (Bio-Rad, 162-0177) membrane using the Transblot Turbo transfer system (Bio-Rad). The blots were stained with Ponceau S to check for efficient protein transfer and were then de-stained using 1× PBS. The blots were then incubated with the appropriate primary antibody dilution, after a blocking step, prepared in 0.25% BSA in 1× PBS, overnight at 4°C. Subsequently, the blots were incubated with the appropriate HRP-conjugated secondary antibody dilution prepared in 5% skim milk powder (GRM1254, HiMedia Laboratories) in 1× PBS, for 1 h at 37°C. The blots were washed with 1× PBS/PBST periodically after each step to remove any residual reagent from prior steps. The blots were developed using an enhanced chemiluminescence substrate (Clarity, Bio-Rad) prior to imaging using a gel documentation system (G-Box, Syngene, UK).  $\beta$ -actin was used as the loading control. Band intensities were calculated using Fiji (Schneider et al., 2012; ImageJ; NIH, Bethesda, MD, USA).

## Microscopy and Vesicle Tracking

For the immunofluorescence experiments, except for the “APP colocalization” experiments, the photomicrographs were acquired using the DeltaVision Elite widefield microscope (GE Healthcare, Chicago, IL, USA) equipped with a 60× oil immersion objective, with the filter sets: FITC, TRITC, and Cy5. Images were processed using DV SoftWoRX software. Fluorescence intensity calculations, corrected according to the area, were performed using Fiji (NIH, Bethesda, MD, USA). For the “APP colocalization” experiments, photomicrographs were acquired using the Zeiss LSM 880 confocal microscope (Carl Zeiss, Germany) equipped with a 63× oil immersion objective, with the filter sets: FITC, TRITC, and Cy5. Colocalization analyses of the photomicrographs were performed using the “Colocalization Analysis” plugin of Fiji (NIH, Bethesda, MD, USA), which provided the corresponding Mander’s overlap data.

For live-cell imaging experiments, movies were acquired using the Zeiss LSM 880 confocal microscope equipped with a climate chamber, wherein frames were acquired every 3 s for 180 s using a 63× oil immersion objective with a zoom of 1.5–2.5. Vesicle tracking, as well as vesicle fusion/fission analyses, were computed using a Fiji plugin—TrackMate (Tinevez et al., 2017). DoG detector of TrackMate was used for segmentation of RAB5-labeled vesicles, and the autothreshold setting of TrackMate was used to select only those vesicles whose fluorescence intensity was sufficiently high with respect to the background fluorescence intensity. Subsequently, the LAP tracker of TrackMate, which uses frame-to-frame linking for the construction of vesicle trajectories, was used for tracking vesicles and monitoring vesicle fusion/fission events. The following configuration was used for LAP tracker: maximum linking distance = 500 nm; maximum gap-closing distance = 500 nm;

maximum frame gap = 2. Merging vesicle trajectories were considered as a vesicle fusion event, whereas a splitting vesicle trajectory was considered as a vesicle fission event. After configuration, TrackMate generates trajectories of the different vesicles in a cell and generates the appropriate data in a “heat-map” format to show the dynamic range of vesicle motility/displacement/fusion/fission as well as the corresponding raw data.

## Statistical Analyses

All data generated are from at least three independent experiments. The number of cells considered for statistics for each experiment is mentioned in the respective figure legend. Statistical analyses for all experiments were performed using the unpaired two-tailed Student’s *t*-test followed by the *post hoc* Bonferroni test, using the GraphPad Prism 6 software (GraphPad Software Inc., San Diego, CA, USA). Grubbs’ test was used to remove any significant outliers ( $p < 0.05$ ) in the experimental data. Error bars represent mean  $\pm$  SEM. A *p*-value of less than 0.05 was considered statistically significant.

## RESULTS

### Expression of Markers Associated With Endolysosomal Dynamics Is Affected Upon 4R0N Tau Overexpression

Prior to the investigation of endolysosomal system dynamics, we first elucidated the expression of specific markers involved in the endolysosomal pathway such as RAB5, RAB7, and LAMP1. Using immunofluorescence, we found that the expression levels of RAB5 ( $p < 0.0001$ ), RAB7 ( $p < 0.05$ ), and LAMP1 ( $p < 0.0001$ ) were significantly upregulated in HeLa cells transiently transfected with 4R0N tau (pRK5-EGFP-tau) compared to HeLa cells transiently transfected with the vector control (pEGFP-N1). Additionally, we determined the expression of beclin-1, a key regulator of endocytic trafficking, early endosome maturation, and autophagy progression (Liang et al., 1999; Lucin et al., 2013; McKnight et al., 2014). The expression level of beclin-1 was found to be significantly downregulated ( $p < 0.0001$ ) in the 4R0N tau-overexpressing cells, compared to those of the control (Figure 1A). These observations were corroborated by immunoblot experiments, which showed a similar trend in the expression levels of these markers (Figure 1B). Further investigation is required to understand some of the observed expression patterns.

### Increased RAB7 Expression Could be Attributed to an Increase in the Number of Autophagic Vacuoles in the Background of 4R0N Tau Overexpression

Unlike RAB5, which typically labels early endosomes, RAB7 labels late endocytic compartments and lysosomes in addition to autophagic vacuoles. Autophagic vacuoles include autophagosomes, amphisomes, and autolysosomes, commonly labeled with the protein marker, LC3; autophagosomes

and amphisomes ultimately mature into autolysosomes (Gutierrez et al., 2004; Jäger et al., 2004; Colacurcio et al., 2018). Hence, the RAB7 readout from the previous immunofluorescence experiment could indicate an increase in either the number of RAB7-labeled endocytic compartments or an increase in the number of RAB7+LC3-labeled autophagic vacuoles. To address this, we cotransfected cells of the control and 4R0N tau groups with pmRFP-LC3 and immunostained for RAB7 to examine the number of autophagic vacuoles. Through this experiment, we observed that the 4R0N tau-overexpressing HeLa cells displayed a significantly higher number of autophagic vacuoles ( $p < 0.01$ ) compared to that of the control cells (Figure 2). Therefore, the initially observed increase in the expression of RAB7 could be indicative of an increase in the number of RAB7+LC3-labeled autophagic vacuoles instead of RAB7-labeled endocytic compartments. The elevated number of autophagic vacuoles in the 4R0N tau-overexpressing cells could be immature due to the reduced expression of beclin-1 observed earlier, potentially

representative of autophagic stress induced by overexpression of 4R0N tau.

### 4R0N Tau Abrogates Maturation and Spatiotemporal Dynamics of Early Endocytic Vesicular Compartments

It is unclear whether the previously observed increase in RAB5 expression is indicative of upregulated or disrupted endocytic flux. To address this, we performed live-cell imaging and vesicular tracking analyses (refer to the “Materials and Methods” section, for more details). It is well known that the homotypic fusion of early endosomes is necessary for their maturation into late endosomes. Consequently, we hypothesized that if endocytic flux was negatively impacted at the maturation stage of early endosomes, then the ratio of vesicle fusion events to vesicle fission events would be altered. To test this hypothesis, live-cell imaging of vector control and 4R0N tau-overexpressing HeLa cells cotransfected with mCh-RAB5 was conducted, to evaluate the number of vesicle fusion and fission events. The

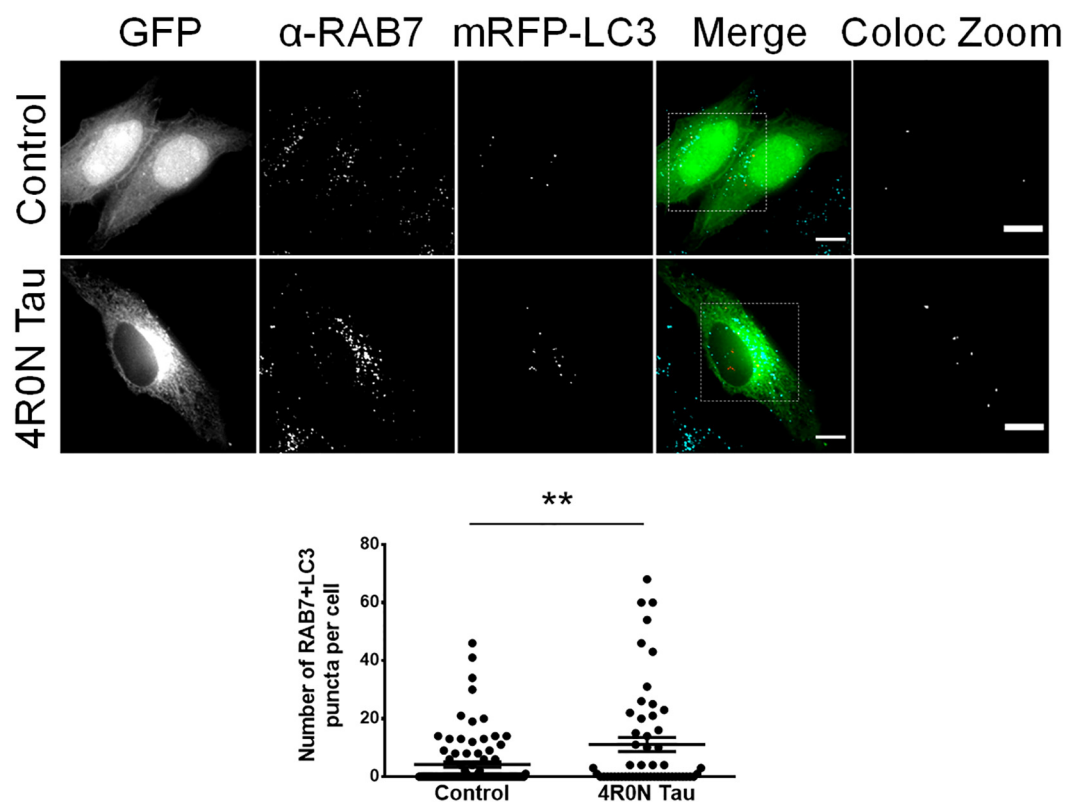


**FIGURE 2 |** Increased number of autophagic vacuoles in HeLa cells overexpressing 4R0N tau. Representative immunofluorescence single z-stack photomicrographs of vector control and 4R0N tau-overexpressing cells cotransfected with the pmRFP-LC3 (mRFP-LC3) construct and immunostained for RAB7 and corresponding statistical data. The signals of the antibody staining, the “GFP” channel, and the “mRFP-LC3” channel are represented in cyan, green, and red, respectively, in the “Merge” channel. The insets in the “Merge” channel are magnified further, and only the RAB7+LC3 (colocalization of mRFP-LC3 puncta with RAB7 puncta) puncta, of both groups, are shown as the “Coloc Zoom” channel, representing the number of autophagic vacuoles. A significant increase in the number of autophagic vacuoles is observed in the 4R0N tau-overexpressing cells. For quantification and statistical analysis, three z-stacks of individual cells were considered ( $N = 20$ – $30$  cells per independent experiment). Statistical analysis was performed using unpaired two-tailed Student’s *t*-test. Scale bar:  $10 \mu\text{m}$ . Error bars reflect mean  $\pm$  SEM,  $**p < 0.01$ .  $n = 3$  independent experiments.

number of RAB5-labeled vesicle fission events ( $p < 0.05$ ) was found to be elevated in 4R0N tau-overexpressing cells compared to that of the control cells, while the number of RAB5-labeled fusion events did not significantly differ in both groups of cells (Figure 3A). Additionally, the ratio of vesicle fusion events to vesicle fission events was significantly less ( $p < 0.001$ ) in the 4R0N tau-overexpressing cells compared to that of the control cells (Figure 3A). These observations hint toward an inherent bias for RAB5-labeled vesicle fission in the 4R0N tau-overexpressing cells. To further understand the differences between the groups, we studied the spatiotemporal aspects of RAB5-labeled vesicles. Overall motility ( $p < 0.001$ ) and displacement ( $p < 0.0001$ ) of RAB5-labeled vesicles were found to be dramatically reduced under 4R0N tau overexpression (Figure 3B). Moreover, the trajectories of the vesicles followed a random pattern compared to that of the vector control cells (Figure 3B), which showed clearly defined trajectories. These data indicate that 4R0N tau hampers the maturation of RAB5-labeled early endocytic compartments and impedes the trafficking of these vesicles. These observations suggest that the previously observed upregulation of RAB5 expression could stem from the disruption of endocytic flux at the early endocytic stage, attributable to 4R0N tau overexpression.

### 4R0N Tau Overexpression Promotes the Sequestration of APP Into Endocytic Compartments

From the previous experiments, we observed that the endocytic vesicular dynamics were affected due to 4R0N tau overexpression. As a consequence, we hypothesized that the trafficking of specific endocytic cargoes could also be affected. Of the many endocytic cargoes, APP piqued our interest due to its implications in AD. In order to elucidate the degree of APP colocalization with markers of the endocytic pathway, we cotransfected the control and 4R0N tau-overexpressing cells with the pDsRedm-C1:APP construct, which encodes APP with a C-terminal DsRed tag. These cells were then immunostained to detect the expression of the respective endolysosomal protein marker. The colocalization channel was used to evaluate the degree of APP colocalization along the endocytic pathway (refer to the Materials and Methods section, for more details). In the 4R0N tau-overexpressing cells, APP was selectively sequestered to RAB5-labeled ( $p < 0.0001$ ) and RAB7-labeled ( $p < 0.05$ ) vesicles (Figure 4). There was no significant difference in the colocalization of APP with LAMP1 (ns; Figure 4) between the two groups of cells. These observations indicate that tau overexpression disrupts the trafficking of APP such that APP accumulates in the endocytic compartments contributing to amyloidogenic processing instead of being delivered to the lysosomal compartments for degradation.

### DISCUSSION

Our investigation revealed that the dynamics of the endolysosomal system and autophagy are compromised upon overexpression of soluble 4R0N tau. We observed that the

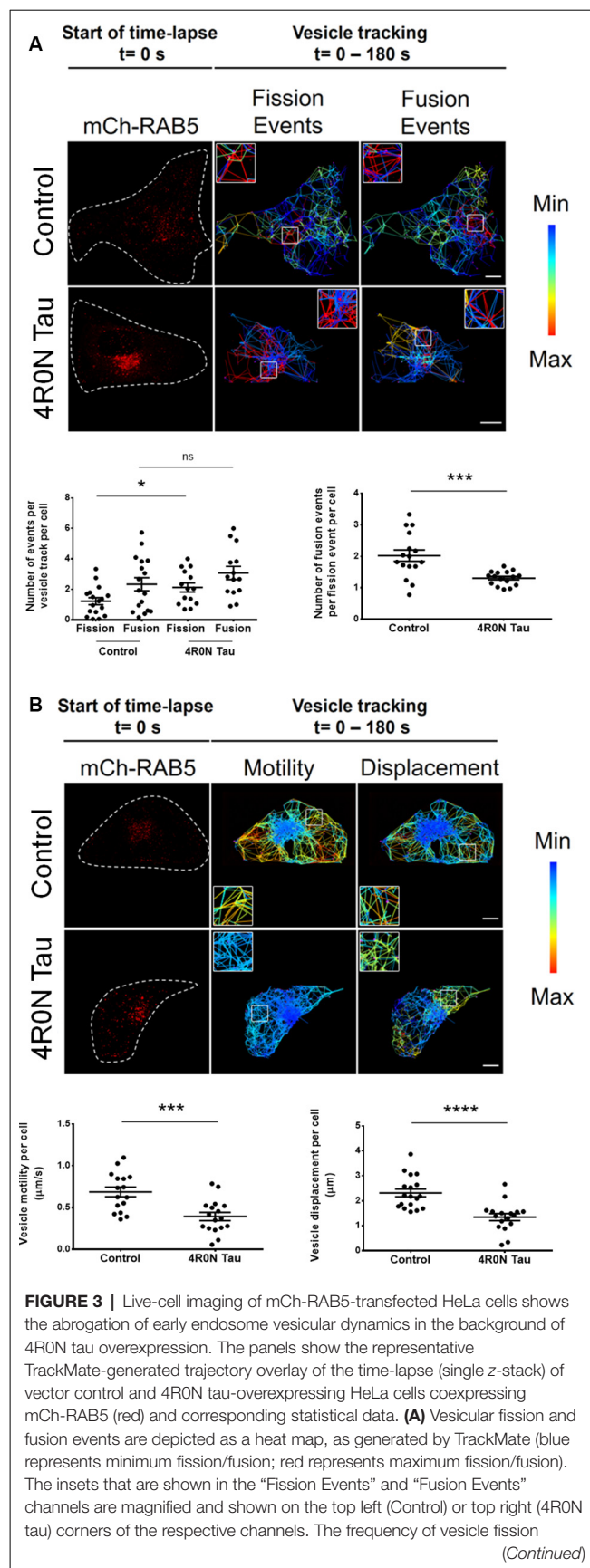


**FIGURE 3 |** Live-cell imaging of mCh-RAB5-transfected HeLa cells shows the abrogation of early endosome vesicular dynamics in the background of 4R0N tau overexpression. The panels show the representative TrackMate-generated trajectory overlay of the time-lapse (single z-stack) of vector control and 4R0N tau-overexpressing HeLa cells coexpressing mCh-RAB5 (red) and corresponding statistical data. (A) Vesicular fission and fusion events are depicted as a heat map, as generated by TrackMate (blue represents minimum fission/fusion; red represents maximum fission/fusion). The insets that are shown in the “Fission Events” and “Fusion Events” channels are magnified and shown on the top left (Control) or top right (4R0N tau) corners of the respective channels. The frequency of vesicle fission (Continued)

**FIGURE 3 |** Continued

events is increased in the 4R0N tau-overexpressing cells, while the frequency of vesicle fusion events does not show a concomitant increase, suggesting an impairment in early endosome maturation. The corresponding graphs depicting the number of fusion and fission events as well as the number of fusion events per fission event of both groups are shown below the panel.

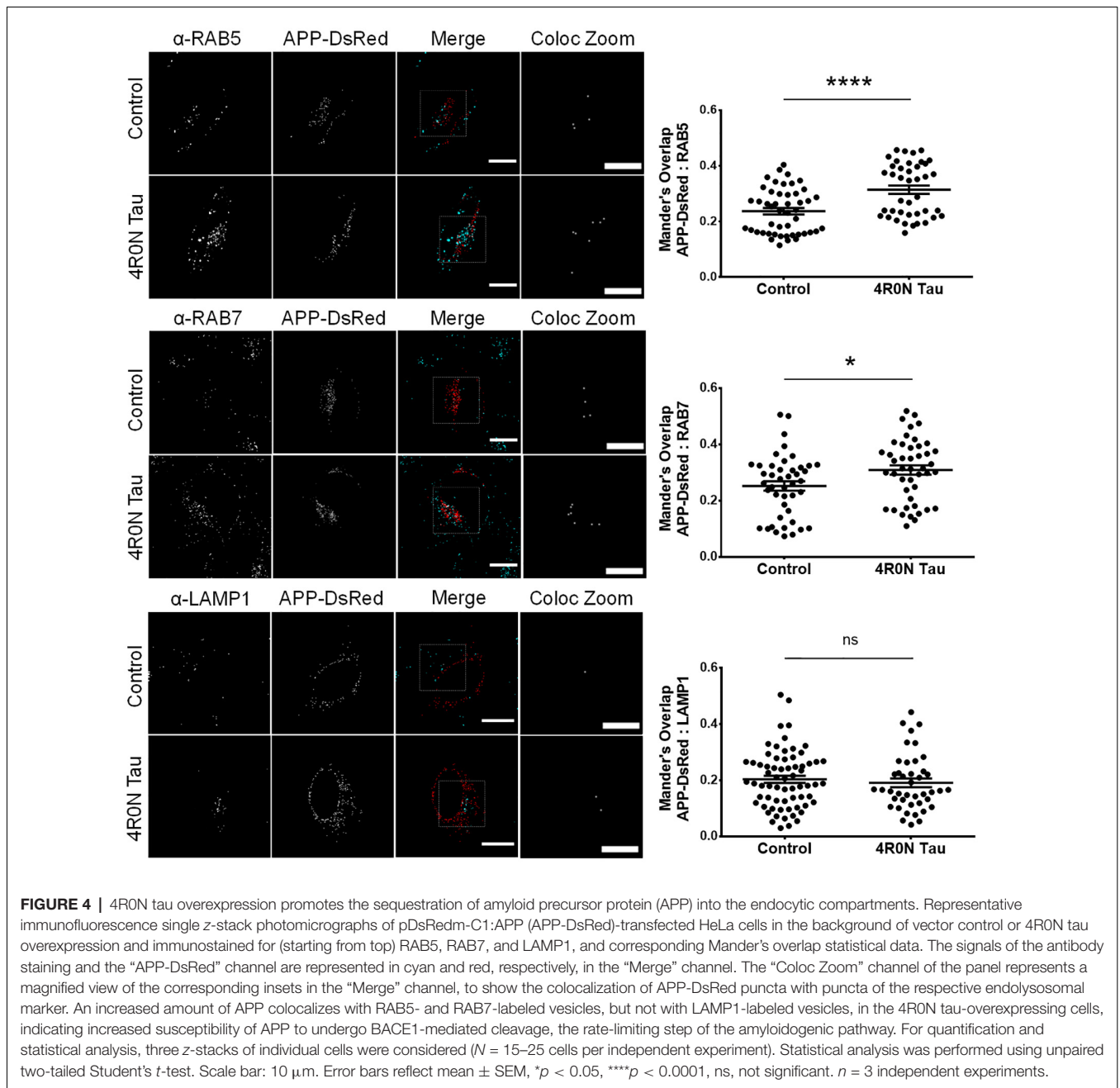
**(B)** The range of vesicle motility and displacement is depicted as a heat map, as generated by TrackMate (blue represents minimum motility/displacement; red represents maximum motility/displacement). The insets shown in the “Motility” and “Displacement” channels are magnified and shown in the bottom left (Control) or top left (4R0N tau) corners of the respective channels. The vesicle motility and displacement of RAB5-labeled vesicles are lower in the 4R0N tau-overexpressing cells. The corresponding graphs depicting the vesicle motility and displacement of both groups are shown below the panel. Vesicles in the 4R0N tau-overexpressing cells follow a random pattern unlike the well-defined pattern of the vesicles in the cells of the vector control group. The vesicular dynamics were tracked for 180 s with frames taken every 3 s. For quantification and statistical analysis, the middle z-stack of individual cells was considered ( $N = 14-19$  cells). White dashed lines demarcate individual cells. Statistical analysis was performed using unpaired two-tailed Student's *t*-test. Scale bar: 10  $\mu$ m. Error bars reflect mean  $\pm$  SEM, \* $p < 0.05$ , \*\*\* $p < 0.001$ , \*\*\*\* $p < 0.0001$ , ns, not significant.  $n = 3$  independent experiments.

expression levels of RAB5, RAB7, and LAMP1 were affected due to soluble 4R0N tau overexpression. These results are in agreement with the AD clinical studies wherein a similar expression profile of these markers was observed (Ginsberg et al., 2010a,b, 2011). Similarly, APP/A $\beta$ -related pathology has also been found to positively regulate the expression levels of RAB5, RAB7, and LAMP1, aside from affecting associated endocytic vesicle morphology (Ji et al., 2006; Cataldo et al., 2008; Kim et al., 2016; Willén et al., 2017). Thus, the primary causative factor responsible for such an expression profile in AD clinical cases remains yet to be identified, but it is worth noting that both tau and A $\beta$ -related pathologies can individually affect the endolysosomal system in similar ways. Studies have reported that RAB5- and RAB7-labeled vesicles are the primary sites of amyloidogenesis in a cell (Haass et al., 2012; Das et al., 2015). Enhanced expression of these RABs could indicate a greater propensity for A $\beta$  production due to an increased pool of endocytic APP resulting in increased amyloidogenesis (Grbovic et al., 2003). We also found that soluble 4R0N tau overexpression leads to decreased beclin-1 expression, which is in agreement with AD-related clinical studies (Rohn et al., 2011; Orr and Oddo, 2013). Beclin-1 regulates autophagy, as well as endocytic trafficking and maturation through its ability to recruit the retromer complex to the endosomal compartments (Liang et al., 1999; Lucin et al., 2013; McKnight et al., 2014). Additionally, it has been shown that beclin-1 can directly regulate APP endocytosis (Swaminathan et al., 2016). Therefore, a deficiency of beclin-1 could potentially impair endocytic trafficking and maturation leading to increased accumulation of APP in the endocytic compartments, thereby increasing the susceptibility of APP to undergo amyloidogenic processing. Furthermore, we observed an increased number of autophagic vacuoles, possibly immature, in the soluble 4R0N tau-overexpressing cells, which could be due to autophagic stress in correlation to beclin-1 deficiency. A similar phenotype has been noted in AD patient

brains, deficient of beclin-1, wherein autophagic vacuoles were shown to be accumulated in dystrophic neurites, unable to fuse with functional lysosomes (Nixon et al., 2005; Li et al., 2010; Tammineni et al., 2017). The observed down-regulation of beclin-1 was concluded to be independent of A $\beta$  pathology since APP transgenic mouse models of AD, based on A $\beta$  pathology, did not exhibit decreased beclin-1 expression levels (Pickford et al., 2008). Overall, these observations support the hypothesis that the pathological effects of tau precede A $\beta$ -associated pathology, with beclin-1 deficiency acting as an intermediary factor responsible for the dysregulation of endolysosomal dynamics and autophagy. Our observations outline a framework in agreement with the outlook of AD-related clinical studies.

The previous conclusion is further strengthened by the colocalization experiments, which aimed to elucidate the localization of APP upon soluble 4R0N tau overexpression. We found that APP was selectively sequestered to RAB5- and RAB7-labeled vesicles. Disruption of endocytic flux is evident since a concomitant increase in the colocalization of APP with LAMP1-labeled lysosomes was not observed. Further, the impaired maturation and trafficking of RAB5-labeled vesicles observed in our study could suggest delayed turnover of early endocytic compartments, which can, in turn, influence the rate of amyloidogenesis since APP is not able to reach the lysosomes for proteolytic degradation. Collectively, the delicate balance between the degradation and amyloidogenic processing of APP is affected due to soluble 4R0N tau overexpression. This leads us to postulate that soluble 4R0N tau pathology could underscore AD pathogenesis through disruption of endolysosomal function, autophagic stress, and enhanced amyloidogenic processing of APP at endocytic compartments, although further research is warranted. However, it must be noted that the mechanistic link between soluble tau overexpression and the reported phenotypes remains elusive, and it should be an important subject for future studies. Based on previous literature, it is plausible that soluble tau could localize in the lumen and/or the membrane of endocytic vesicles (Vaz-Silva et al., 2018), and interact with ESCRT machinery-associated proteins potentially leading to dysfunction of the ESCRT pathway, which is associated with impaired endosomal trafficking and function (Watson et al., 2015; Oshima et al., 2016). Further experimentation is required to unequivocally establish the mode of soluble tau pathology that causes the phenotypes observed in our study, owing to soluble 4R0N tau overexpression. Furthermore, it is important to note that the observations reported in our study must be validated with other appropriate models, and hence, it must be interpreted with caution.

The model proposed by our study is in line with documented AD clinical observations. Biomarker studies based on cerebrospinal fluid (CSF) and neuropathological analysis of AD clinical cases have revealed a specific temporal pattern of accumulation of pathological proteins. To substantiate, while it has been shown that reduction of A $\beta$  protein levels in the CSF precedes that of tau aggregates by many years, the accumulation of tau with AD relevant phosphorylation epitopes takes place decades before A $\beta$  plaque formation (Motter et al., 1995; Braak et al., 2011, 2013; Musiek and Holtzman, 2012).



Moreover, fibrillary A $\beta$  and tau pathologies were found to be spatiotemporally disconnected within the human central nervous system (Thal et al., 2000; Braak et al., 2006). Such a disconnect between the fibrillary versions of the two critical biomarkers of AD, A $\beta$  and tau, makes it unclear as to which biomarker of AD takes precedence. More importantly, it questions the very idea of a physiological cross-talk between A $\beta$  and tau that leads to pathology. Contrastingly, the soluble forms of tau and A $\beta$  show a much better overlap of neuropathological association in the temporal lobe of the AD brain, and this cross-talk event occurs before their terminal state as fibrillary counterparts are observed in a similar location (Koss et al., 2016). Therefore, from a clinical

standpoint, it has been demonstrated that the soluble forms of A $\beta$  and tau can cross-talk prior to aggregation. This critical period, before the nucleation of aggregates, requires further investigation to firmly establish the sequence of events that connect the pathologies of A $\beta$  and tau. In this regard, our study has found a possible mode of cross-talk between tau and A $\beta$ .

To conclude, our study has revealed the pathological profile of soluble 4R0N tau overexpression in cells, which recapitulates some of the earliest phenotypes observed in AD clinical cases such as endolysosomal dysfunction and autophagic stress (Orr and Oddo, 2013; Whyte et al., 2017; Colacurcio et al., 2018). The impaired dynamics of the endolysosomal system have

serious implications in the generation of A $\beta$ . With several AD clinical trials targeting aggregated tau, our findings enforce the notion that therapeutic intervention must be focused on soluble tau pathology.

## DATA AVAILABILITY STATEMENT

All datasets generated for this study are included in the article.

## AUTHOR CONTRIBUTIONS

RM, SS, and TM designed the study. LG provided technical support and helped with the cell culture experiments. SS and TM analyzed the data. RM, SS, and TM interpreted the findings of the study. TM performed the experiments and prepared the final manuscript, which was critically reviewed by all the other authors. All authors contributed to the article and approved the submitted version.

## REFERENCES

- Ambadipudi, S., Biernat, J., Riedel, D., Mandelkow, E., and Zweckstetter, M. (2017). Liquid-liquid phase separation of the microtubule-binding repeats of the Alzheimer-related protein tau. *Nat. Commun.* 8:275. doi: 10.1038/s41467-017-00480-0
- Bolós, M., Pallas-Bazarra, N., Terreros-Roncal, J., Perea, J. R., Jurado-Arjona, J., Ávila, J., et al. (2017). Soluble tau has devastating effects on the structural plasticity of hippocampal granule neurons. *Transl. Psychiatry* 7:1267. doi: 10.1038/s41398-017-0013-6
- Braak, H., Alafuzoff, I., Arzberger, T., Kretschmar, H., and Del Tredici, K. (2006). Staging of Alzheimer disease-associated neurofibrillary pathology using paraffin sections and immunocytochemistry. *Acta Neuropathol.* 112, 389–404. doi: 10.1007/s00401-006-0127-z
- Braak, H., Thal, D. R., Ghebremedhin, E., and Del Tredici, K. (2011). Stages of the pathologic process in Alzheimer disease: age categories from 1 to 100 years. *J. Neuropathol. Exp. Neurol.* 70, 960–969. doi: 10.1097/NEN.0b013e318232a379
- Braak, H., Zetterberg, H., Del Tredici, K., and Blennow, K. (2013). Intraneuronal tau aggregation precedes diffuse plaque deposition, but amyloid- $\beta$  changes occur before increases of tau in cerebrospinal fluid. *Acta Neuropathol.* 126, 631–641. doi: 10.1007/s00401-013-1139-0
- Busche, M. A., Wegmann, S., Dujardin, S., Commins, C., Schiantarelli, J., Klickstein, N., et al. (2019). Tau impairs neural circuits, dominating amyloid- $\beta$  effects, in Alzheimer models *in vivo*. *Nat. Neurosci.* 22, 57–64. doi: 10.1038/s41593-018-0289-8
- Cataldo, A. M., Mathews, P. M., Boiteau, A. B., Hassinger, L. C., Peterhoff, C. M., Jiang, Y., et al. (2008). Down syndrome fibroblast model of Alzheimer-related endosome pathology: accelerated endocytosis promotes late endocytic defects. *Am. J. Pathol.* 173, 370–384. doi: 10.2353/ajpath.2008.071053
- Colacurcio, D. J., Pensalfini, A., Jiang, Y., and Nixon, R. A. (2018). Dysfunction of autophagy and endosomal-lysosomal pathways: roles in pathogenesis of down syndrome and Alzheimer's disease. *Free Radic. Biol. Med.* 114, 40–51. doi: 10.1016/j.freeradbiomed.2017.10.001
- Crowther, R., Olesen, O., Smith, M., Jakes, R., and Goedert, M. (1994). Assembly of Alzheimer-like filaments from full-length tau protein. *FEBS Lett.* 337, 135–138. doi: 10.1016/0014-5793(94)80260-2

## FUNDING

This study was supported by JNCASR intramural funds, DST—Science and Engineering Research Board (SERB) grant (EMR/2015/001946), Department of Biotechnology grant in Life Science Research, Education and Training at JNCASR (BT/INF/22/SP27679/2018), and DST-SERB [SR/WOS-A/LS-1249/2015(G)].

## ACKNOWLEDGMENTS

We thank Prof. Erika Holzbaur for the pDsRedm-C1:APP plasmid. We thank members of the Autophagy Laboratory, JNCASR, for their support and guidance throughout the project. We thank Aparna Hebbar, Akshaya Nambiar, and Mridhula Giridharan for the critical reading of the manuscript. We thank Sreedevi Padmanabhan and Pavani Rekulapalli for the technical help with experimental procedures. We thank B. Suma for the confocal microscopy, JNCASR. We thank the reviewers for their constructive criticisms, which helped in improving the manuscript significantly.

- Das, U., Wang, L., Ganguly, A., Saikia, J. M., Wagner, S. L., Koo, E. H., et al. (2015). Visualizing APP and BACE-1 approximation in neurons yields insight into the amyloidogenic pathway. *Nat. Neurosci.* 19, 55–64. doi: 10.1038/nn.4188
- Dai, C.-L., Tung, Y. C., Liu, F., Gong, C.-X., and Iqbal, K. (2017). Tau passive immunization inhibits not only tau but also Abeta pathology. *Alzheimers Res. Ther.* 9:1. doi: 10.1186/s13195-016-0227-5
- Dawson, T. M., Golde, T. E., and Lagier-Tourenne, C. (2018). Animal models of neurodegenerative diseases. *Nat. Neurosci.* 21, 1370–1379. doi: 10.1038/s41593-018-0236-8
- de Calignon, A., Fox, L. M., Pitstick, R., Carlson, G. A., Bacskai, B. J., Spires-Jones, T. L., et al. (2010). Caspase activation precedes and leads to tangles. *Nature* 464, 1201–1204. doi: 10.1038/nature08890
- Friedman, J. R., Webster, B. M., Mastronarde, D. N., Verhey, K. J., and Voeltz, G. K. (2010). ER sliding dynamics and ER-mitochondrial contacts occur on acetylated microtubules. *J. Cell. Biol.* 190, 363–375. doi: 10.1083/jcb.200911024
- Fu, M.-M., and Holzbaur, E. L. F. (2013). JIP1 regulates the directionality of APP axonal transport by coordinating kinesin and dynein motors. *J. Cell Biol.* 202, 495–508. doi: 10.1083/jcb.201302078
- Ginsberg, S. D., Alldred, M. J., Counts, S. E., Cataldo, A. M., Neve, R. L., Jiang, Y., et al. (2010a). Microarray analysis of hippocampal CA1 neurons implicates early endosomal dysfunction during Alzheimer's disease progression. *Biol. Psychiatry* 68, 885–893. doi: 10.1016/j.biopsych.2010.05.030
- Ginsberg, S. D., Mufson, E. J., Alldred, M. J., Counts, S. E., Wu, J., Nixon, R. A., et al. (2011). Upregulation of select rab GTPases in cholinergic basal forebrain neurons in mild cognitive impairment and Alzheimer's disease. *J. Chem. Neuroanat.* 42, 102–110. doi: 10.1016/j.jchemneu.2011.05.012
- Ginsberg, S. D., Mufson, E. J., Counts, S. E., Wu, J., Alldred, M. J., Nixon, R. A., et al. (2010b). Regional selectivity of rab5 and rab7 protein upregulation in mild cognitive impairment and Alzheimer's disease. *J. Alzheimers Dis.* 22, 631–639. doi: 10.3233/JAD-2010-101080
- Grbovic, O. M., Mathews, P. M., Jiang, Y., Schmidt, S. D., Dinakar, R., Summers-Terio, N. B., et al. (2003). Rab5-stimulated up-regulation of the endocytic pathway increases intracellular  $\beta$ -cleaved amyloid precursor protein carboxyl-terminal fragment levels and A $\beta$  production. *J. Biol. Chem.* 278, 31261–31268. doi: 10.1074/jbc.M304122200
- Gutierrez, M. G., Munafó, D. B., Berón, W., and Colombo, M. I. (2004). Rab7 is required for the normal progression of the autophagic pathway in mammalian cells. *J. Cell Sci.* 117, 2687–2697. doi: 10.1242/jcs.01114

- Haass, C., Kaether, C., Thinakaran, G., and Sisodia, S. (2012). Trafficking and proteolytic processing of APP. *Cold Spring Harb. Perspect. Med.* 2:a006270. doi: 10.1101/cshperspect.a006270
- He, H. J., Wang, X. S., Pan, R., Wang, D. L., Liu, M. N., and He, R. Q. (2009). The proline-rich domain of tau plays a role in interactions with actin. *BMC Cell Biol.* 10:81. doi: 10.1186/1471-2121-10-81
- Hoover, B. R., Reed, M. N., Su, J., Penrod, R. D., Kotilinek, L. A., Grant, M. K., et al. (2010). Tau mislocalization to dendritic spines mediates synaptic dysfunction independently of neurodegeneration. *Neuron* 68, 1067–1081. doi: 10.1016/j.neuron.2010.11.030
- Ittner, L. M., Ke, Y. D., Delerue, F., Bi, M., Gladbach, A., van Eersel, J., et al. (2010). Dendritic function of tau mediates amyloid- $\beta$  toxicity in Alzheimer's disease mouse models. *Cell* 142, 387–397. doi: 10.1016/j.cell.2010.06.036
- Jäger, S., Bucci, C., Tanida, I., Ueno, T., Kominami, E., Saftig, P., et al. (2004). Role for Rab7 in maturation of late autophagic vacuoles. *J. Cell Sci.* 117, 4837–4848. doi: 10.1242/jcs.01370
- Ji, Z.-S., Müllendorff, K., Cheng, I. H., Miranda, R. D., Huang, Y., and Mahley, R. W. (2006). Reactivity of apolipoprotein E4 and amyloid  $\beta$  peptide: lysosomal stability and neurodegeneration. *J. Biol. Chem.* 281, 2683–2692. doi: 10.1074/jbc.M506646200
- Johnson, K. A., Schultz, A., Betensky, R. A., Becker, J. A., Sepulcre, J., Rentz, D., et al. (2016). Tau positron emission tomographic imaging in aging and early Alzheimer disease. *Ann. Neurol.* 79, 110–119. doi: 10.1002/ana.24546
- Khatoun, S., Grundke-Iqbal, I., and Iqbal, K. (1992). Brain levels of microtubule-associated protein  $\tau$  are elevated in Alzheimer's disease: a radioimmunoslot-blot assay for nanograms of the protein. *J. Neurochem.* 59, 750–753. doi: 10.1111/j.1471-4159.1992.tb09432.x
- Kim, S., Sato, Y., Mohan, P. S., Peterhoff, C., Pensalfini, A., Rigoglioso, A., et al. (2016). Evidence that the rab5 effector APPL1 mediates APP- $\beta$ CTF-induced dysfunction of endosomes in down syndrome and Alzheimer's disease. *Mol. Psychiatry* 21, 707–716. doi: 10.1038/mp.2015.97
- Kimura, S., Noda, T., and Yoshimori, T. (2007). Dissection of the autophagosome maturation process by a novel reporter protein, tandem fluorescent-tagged LC3. *Autophagy* 3, 452–460. doi: 10.4161/auto.4451
- Koss, D. J., Jones, G., Cranston, A., Gardner, H., Kanaan, N. M., and Platt, B. (2016). Soluble pre-fibrillar tau and  $\beta$ -amyloid species emerge in early human Alzheimer's disease and track disease progression and cognitive decline. *Acta Neuropathol.* 132, 875–895. doi: 10.1007/s00401-016-1632-3
- Li, L., Zhang, X., and Le, W. (2010). Autophagy dysfunction in Alzheimer's disease. *Neurodegener. Dis.* 7, 265–271. doi: 10.1159/000276710
- Liang, X. H., Jackson, S., Seaman, M., Brown, K., Kempkes, B., Hibshoosh, H., et al. (1999). Induction of autophagy and inhibition of tumorigenesis by beclin 1. *Nature* 402, 672–676. doi: 10.1038/45257
- Lucin, K. M., O'Brien, C. E., Bieri, G., Czirr, E., Mosher, K. I., Abbey, R. J., et al. (2013). Microglial beclin 1 regulates retromer trafficking and phagocytosis and is impaired in Alzheimer's disease. *Neuron* 79, 873–886. doi: 10.1016/j.neuron.2013.06.046
- Maeda, S., Sahara, N., Saito, Y., Murayama, S., Ikai, A., and Takashima, A. (2006). Increased levels of granular tau oligomers: an early sign of brain aging and Alzheimer's disease. *Neurosci. Res.* 54, 197–201. doi: 10.1016/j.neures.2005.11.009
- Mandelkow, E. M., and Mandelkow, E. (2012). Biochemistry and cell biology of tau protein in neurofibrillary degeneration. *Cold Spring Harb. Perspect. Med.* 2:a006247. doi: 10.1101/cshperspect.a006247
- McGowan, E., Eriksen, J., and Hutton, M. (2006). A decade of modeling Alzheimer's disease in transgenic mice. *Trends Genet.* 22, 281–289. doi: 10.1016/j.tig.2006.03.007
- McKnight, N. C., Zhong, Y., Wold, M. S., Gong, S., Phillips, G. R., Dou, Z., et al. (2014). Beclin 1 is required for neuron viability and regulates endosome pathways via the UVRAG-VPS34 complex. *PLoS Genet.* 10:e1004626. doi: 10.1371/journal.pgen.1004626
- Mitchell, T. W., Mufson, E. J., Schneider, J. A., Cochran, E. J., Nissanov, J., Han, L.-Y., et al. (2002). Parahippocampal tau pathology in healthy aging, mild cognitive impairment and early Alzheimer's disease. *Ann. Neurol.* 51, 182–189. doi: 10.1002/ana.10086
- Morris, M., Maeda, S., Vossel, K., and Mucke, L. (2011). The many faces of tau. *Neuron* 70, 410–426. doi: 10.1016/j.neuron.2011.04.009
- Motter, R., Vigo-Pelfrey, C., Kholodenko, D., Barbour, R., Johnson-Wood, K., Galasko, D., et al. (1995). Reduction of beta-amyloid peptide42 in the cerebrospinal fluid of patients with Alzheimer's disease. *Ann. Neurol.* 38, 643–648. doi: 10.1002/ana.410380413
- Musiek, E. S., and Holtzman, D. M. (2012). Origins of Alzheimer's disease: reconciling cerebrospinal fluid biomarker and neuropathology data regarding the temporal sequence of amyloid-beta and tau involvement. *Curr. Opin. Neurol.* 25, 715–720. doi: 10.1097/WCO.0b013e32835a30f4
- Nixon, R. A. (2005). Endosome function and dysfunction in Alzheimer's disease and other neurodegenerative diseases. *Neurobiol. Aging* 26, 373–382. doi: 10.1016/j.neurobiolaging.2004.09.018
- Nixon, R. A., Wegiel, J., Kumar, A., Yu, W. H., Peterhoff, C., Cataldo, A., et al. (2005). Extensive involvement of autophagy in Alzheimer disease: an immuno-electron microscopy study. *J. Neuropathol. Exp. Neurol.* 64, 113–122. doi: 10.1093/jnen/64.2.113
- Orr, M. E., and Oddo, S. (2013). Autophagic/lysosomal dysfunction in Alzheimer's disease. *Alzheimers Res. Ther.* 5:53. doi: 10.1186/alzrt217
- Oshima, R., Hasegawa, T., Tamai, K., Sugeno, N., Yoshida, S., Kobayashi, J., et al. (2016). ESCRT-0 dysfunction compromises autophagic degradation of protein aggregates and facilitates ER stress-mediated neurodegeneration via apoptotic and necroptotic pathways. *Sci. Rep.* 6:24997. doi: 10.1038/srep24997
- Overly, C. C., and Hollenbeck, P. J. (1996). Dynamic organization of endocytic pathways in axons of cultured sympathetic neurons. *J. Neurosci.* 16, 6056–6064. doi: 10.1523/JNEUROSCI.16-19-06056.1996
- Parton, R. G., Simons, K., and Dotti, C. G. (1992). Axonal and dendritic endocytic pathways in cultured neurons. *J. Cell. Biol.* 119, 123–137. doi: 10.1083/jcb.119.1.123
- Patterson, K. R., Remmers, C., Fu, Y., Brooker, S., Kanaan, N. M., Vana, L., et al. (2011). Characterization of prefibrillar tau oligomers *in vitro* and in Alzheimer disease. *J. Biol. Chem.* 286, 23063–23076. doi: 10.1074/jbc.M111.237974
- Pickford, F., Masliah, E., Britschgi, M., Lucin, K., Narasimhan, R., Jaeger, P. A., et al. (2008). The autophagy-related protein beclin 1 shows reduced expression in early Alzheimer disease and regulates amyloid  $\beta$  accumulation in mice. *J. Clin. Invest.* 118, 2190–2199. doi: 10.1172/JCI33585
- Rajendran, L., Honsho, M., Zahn, T. R., Keller, P., Geiger, K. D., Verkade, P., et al. (2006). Alzheimer's disease  $\beta$ -amyloid peptides are released in association with exosomes. *Proc. Natl. Acad. Sci. U S A* 103, 11172–11177. doi: 10.1073/pnas.0603838103
- Roberson, E. D., Scearce-Levie, K., Palop, J. J., Yan, F., Cheng, I. H., Wu, T., et al. (2007). Reducing endogenous tau ameliorates amyloid beta-induced deficits in an Alzheimer's disease mouse model. *Science* 316, 750–754. doi: 10.1126/science.1141736
- Rohn, T. T., Wirawan, E., Brown, R. J., Harris, J. R., Masliah, E., and Vandenabeele, P. (2011). Depletion of Beclin-1 due to proteolytic cleavage by caspases in the Alzheimer's disease brain. *Neurobiol. Dis.* 43, 68–78. doi: 10.1016/j.nbd.2010.11.003
- Santacruz, K., Lewis, J., Spires, T., Kotilinek, L., Ingelsson, M., et al. (2005). Tau suppression in a neurodegenerative mouse model improves memory function. *Science* 309, 476–481. doi: 10.1126/science.1113694
- Schneider, C. A., Rasband, W. S., and Eliceiri, K. W. (2012). NIH image to ImageJ: 25 years of image analysis. *Nat. Methods* 9, 671–675. doi: 10.1038/nmeth.2089
- Schöll, M., Lockhart, S. N., Schonhaut, D. R., O'Neil, J. P., Janabi, M., Ossenkoppele, R., et al. (2016). PET imaging of tau deposition in the aging human brain. *Neuron* 89, 971–982. doi: 10.1016/j.neuron.2016.01.028
- Spires-Jones, T. L., de Calignon, A., Matsui, T., Zehr, C., Pitsstick, R., Wu, H. Y., et al. (2008). *In vivo* imaging reveals dissociation between caspase activation and acute neuronal death in tangle-bearing neurons. *J. Neurosci.* 28, 862–867. doi: 10.1523/JNEUROSCI.3072-08.2008
- Strang, K. H., Croft, C. L., Sorrentino, Z. A., Chakrabarty, P., Golde, T. E., and Giasson, B. I. (2018). Distinct differences in prion-like seeding and aggregation between tau protein variants provide mechanistic insights into tauopathies. *J. Biol. Chem.* 293, 2408–2421. doi: 10.1074/jbc.M117.815357
- Swaminathan, G., Zhu, W., and Plowey, E. D. (2016). BECN1/beclin 1 sorts cell-surface APP/amyloid  $\beta$  precursor protein for lysosomal degradation. *Autophagy* 12, 2404–2419. doi: 10.1080/15548627.2016.1234561
- Tammineni, P., Ye, X., Feng, T., Aikal, D., and Cai, Q. (2017). Impaired retrograde transport of axonal autophagosomes contributes to autophagic stress in Alzheimer's disease neurons. *eLife* 6:e21776. doi: 10.7554/eLife.21776

- Thal, D. R., Rub, U., Schultz, C., Sassin, I., Ghebremedhin, E., Del Tredici, K., et al. (2000). Sequence of abeta-protein deposition in the human medial temporal lobe. *J. Neuropathol. Exp. Neurol.* 59, 733–748. doi: 10.1093/jnen/59.8.733
- Thul, P. J., Åkesson, L., Wiking, M., Mahdessian, D., Geladaki, A., Ait Blal, H., et al. (2017). A subcellular map of the human proteome. *Science* 356:eaal3321. doi: 10.1126/science.aal3321
- Tinevez, J.-Y., Perry, N., Schindelin, J., Hoopes, G. M., Reynolds, G. D., Laplantine, E., et al. (2017). Trackmate: an open and extensible platform for single-particle tracking. *Methods* 115, 80–90. doi: 10.1016/j.ymeth.2016.09.016
- Vaz-Silva, J., Gomes, P., Jin, Q., Zhu, M., Zhuravleva, V., Quintremil, S., et al. (2018). Endolysosomal degradation of tau and its role in glucocorticoid-driven hippocampal malfunction. *EMBO J.* 37:e99084. doi: 10.15252/embj.2018.99084
- Watson, J. A., Bhattacharyya, B. J., Vaden, J. H., Wilson, J. A., Icyuz, M., Howard, A. D., et al. (2015). Motor and sensory deficits in the teetering mice result from mutation of the ESCRT Component HGS. *PLoS Genet.* 11:e1005290. doi: 10.1371/journal.pgen.1005290
- Wegmann, S., Eftekharzadeh, B., Tepper, K., Zoltowska, K. M., Bennett, R. E., Dujardin, S., et al. (2018). Tau protein liquid-liquid phase separation can initiate tau aggregation. *EMBO J.* 37:e98049. doi: 10.15252/embj.201798049
- Weingarten, M. D., Lockwood, A. H., Hwo, S. Y., and Kirschner, M. W. (1975). A protein factor essential for microtubule assembly. *Proc. Natl. Acad. Sci. U S A* 72, 1858–1862. doi: 10.1073/pnas.72.5.1858
- Whyte, L. S., Lau, A. A., Hemsley, K. M., Hopwood, J. J., and Sargeant, T. J. (2017). Endo-lysosomal and autophagic dysfunction: a driving factor in Alzheimer's disease? *J. Neurochem.* 140, 703–717 doi: 10.1111/jnc.13935
- Wille, H., Drewes, G., Biernat, J., Mandelkow, E.-M., and Mandelkow, E. (1992). Alzheimer-like paired helical filaments and antiparallel dimers formed from microtubule-associated protein tau *in vitro*. *J. Cell Biol.* 118, 573–584. doi: 10.1083/jcb.118.3.573
- Willén, K., Edgar, J. R., Hasegawa, T., Tanaka, N., Futter, C. E., and Gouras, G. K. (2017). A $\beta$  accumulation causes MVB enlargement and is modelled by dominant negative VPS4A. *Mol. Neurodegener.* 12:61. doi: 10.1186/s13024-017-0203-y
- Wilson, D. M., and Binder, L. I. (1995). Polymerization of microtubule-associated protein tau under near-physiological conditions. *J. Biol. Chem.* 270, 24306–24314. doi: 10.1074/jbc.270.41.24306
- Zhang, Z., Li, X.-G., Wang, Z.-H., Song, M., Yu, S. P., Kang, S. S., et al. (2018).  $\delta$ -secretase-cleaved tau stimulates A $\beta$  production *via* upregulating STAT1-BACE1 signaling in Alzheimer's disease. *Mol. Psychiatry* doi: 10.1038/s41380-018-0286-z [Epub ahead of Print].

**Conflict of Interest:** The authors declare that the research was conducted in the absence of any commercial or financial relationships that could be construed as a potential conflict of interest.

Copyright © 2020 Mahendran, Suresh, Garimella and Manjithaya. This is an open-access article distributed under the terms of the Creative Commons Attribution License (CC BY). The use, distribution or reproduction in other forums is permitted, provided the original author(s) and the copyright owner(s) are credited and that the original publication in this journal is cited, in accordance with accepted academic practice. No use, distribution or reproduction is permitted which does not comply with these terms.